CRYSTAL GROWTH & DESIGN

Communication

pubs.acs.org/crystal

Spontaneous Growth of Magnesium Hydroxide Fibers at Ambient Conditions

Amir Gheisi,[†] Andreas Sternig,[†] Mojca Rangus,[‡,#] Günther Redhammer,[§] Martin Hartmann,*[,‡] and Oliver Diwald*[,†,§]

[†]Friedrich-Alexander-Universität Erlangen-Nürnberg, [‡]Erlangen Catalysis Resource Center, Universität Erlangen-Nürnberg, Erlangen, Germany

[§]Department of Materials Science and Physics, Paris-Lodron University Salzburg, Salzburg, Austria

Supporting Information

ABSTRACT: Spontaneous transformation paths of nanomaterials point to guiding principles for synthesis. We describe the room temperature transformation of MgO nanocubes into $Mg_3(OH)_5Cl{\cdot}4H_2O$ nanofibers in air and investigated the underlying formation mechanism using electron microscopy, X-ray diffraction, and solid-state NMR spectroscopy. Upon contact with water vapor, the magnesium hydroxide needles were found to grow out of agglomerates of highly dispersed MgO nanocubes with preadsorbed $SiCl_4$. Corresponding one-dimensional nanostructures do not form on low surface area materials. The presented growth approach is potentially extendable to other hydrolyzable metal oxides at ultrafine dispersion.

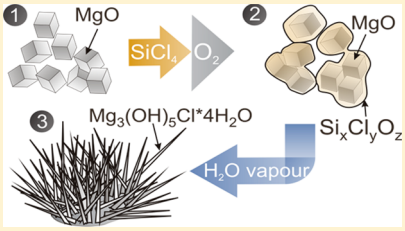

Spontaneous transformations of nanostructures are key to their chemical synthesis and application for two reasons: first, the underlying mechanisms may provide guiding principles for the synthesis and controlled spatial arrangement of anisotropic nanostructures.[1−4] Second, knowledge about the transformation behavior of nanomaterials in the environment is needed in order to reliably assess the potential risk to biological systems. Depending on the nature of particle surfaces and their interactions with gases in the atmosphere, disperse systems can undergo completely changed interfacial chemistries with altered reaction networks as compared to bulk materials.[5]

MgO nanocubes are excellent model systems for surface chemistry studies on unsupported nanomaterials.[6,7] At the same time, they are well-suited building blocks for pure and composite nanostructures.[8,9] We investigated different approaches for $SiCl_4$ adsorption on related particle ensembles (Supporting Information) and discovered an unprecedented transformation process at ambient conditions. The following combined electron microscopy and diffraction study was performed to explore the underlying mechanism. A dry powder of MgO nanoparticles which was casted on the SEM grid can be characterized as agglomerates exhibiting a fine-grained particulate structure.[10] The high dispersion results from the MgO nanocrystals of cubic morphology and an average edge length of approximately 6 nm.

MgO nanocubes exhibit a periclase structure and are phase pure (Figure 1, d1). The relatively broad diffraction features are related to the limited crystalline domain sizes ($d \approx 6$ nm). After 3 days of sample contact with water-saturated air ($p(H_2O) = 32$ mbar) at room temperature, MgO nanocubes were quantitatively converted into the brucite phase (Figure 1, d2) according to

$$MgO + H_2O \rightarrow Mg(OH)_2 \quad (1)$$

From the widths of the diffraction features, we determined for the crystallite dimensions x_{001} and x_{110} coherence lengths of 5 and 10 nm, respectively, using the Scherrer equation. This is in good agreement with the platelike morphology reported of brucite nanocrystals.[11,12] In the case of MgO which was previously contacted with $SiCl_4$ and O_2 and exposed to water vapor thereafter, the material was converted into a solid that is characterized by an entirely different X-ray diffraction (XRD) pattern (Figure 1, d4). Phase analysis on the basis of pattern indexing and lattice parameter refinement led to the compound $Mg_3(OH)_5Cl{\cdot}4H_2O$, thereby closely matching the PDF database card #7-420.[13] The refined cell parameters and atomic coordinates were determined by Rietveld refinement of the powder XRD and are summarized in Table S1 (Supporting Information).

The transformation of MgO into $Mg(OH)_2$ and $Mg_3(OH)_5Cl{\cdot}4H_2O$ needles can also be tracked by ^{25}Mg NMR spectroscopy. A narrow resonance at 26.0 ppm as observed for MgO nanocubes reveals a well-ordered Mg environment without defects and impurities (Figure 2a). Exposure to water vapor triggers the reaction described in eq 1, and the ^{25}Mg NMR spectrum shows broad quadrupolar resonance line (δ = 13 ppm, C_Q = 3.0 MHz, η_Q = 0) characteristic for $Mg(OH)_2$ (Figure 2b).[14−16] The spectrum also indicates a residual small fraction of MgO. The single magnesium resonance observed for the chlorinated MgO powder which was stored in a vacuum (Figure 2c) indicates

Received: April 18, 2014
Revised: July 22, 2014
Published: July 30, 2014

dx.doi.org/10.1021/cg500538d | *Cryst. Growth Des.* 2014, 14, 4236−4239

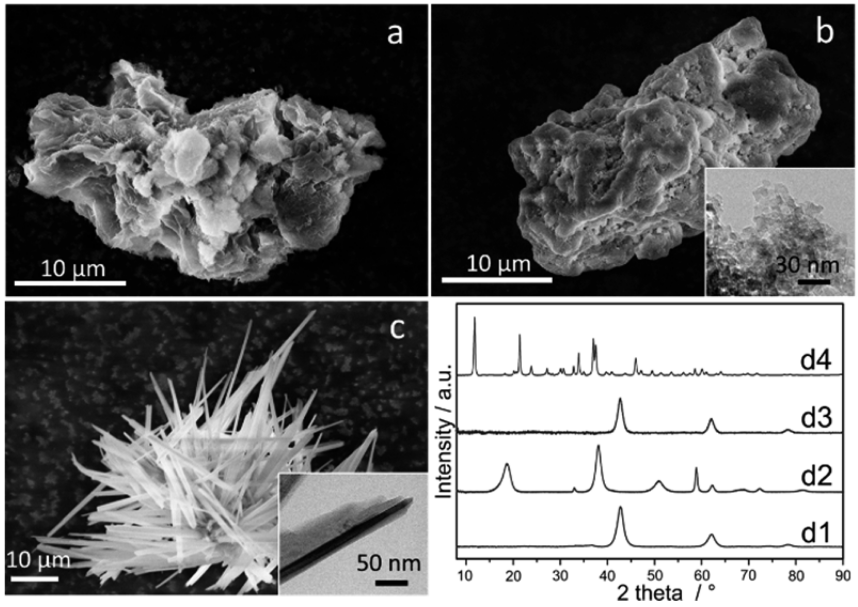

Figure 1. (a) SEM image of a MgO nanocubes agglomerate after room temperature storage in humid air ($p(H_2O)$ = 32 mbar); (b) SEM and TEM images of MgO nanocubes after contact with $SiCl_4$ and subsequent room temperature storage in vacuum ($p < 10^{-5}$ mbar). Additional TEM images are shown in the Supporting Information. (c) EM images of $SiCl_4$ contacted MgO nanocubes after room temperature storage in humid air; (d) X-ray diffraction patterns of (d1) MgO nanocubes, (d2) MgO nanocubes after storage in humid air; (d3) MgO after $SiCl_4/O_2$ contact and storage in a vacuum ($p < 10^{-5}$ mbar), and (d4) $SiCl_4$ contacted MgO nanocubes kept in humid air. In all experiments, the room temperature storage time was 14 days.

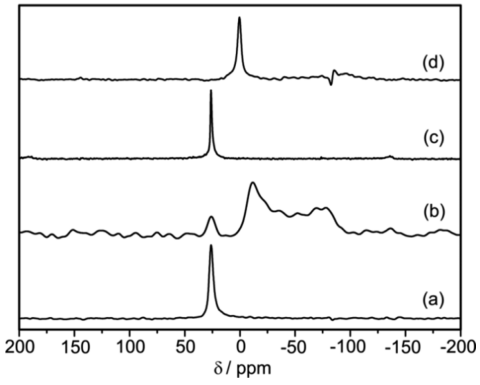

Figure 2. Solid state single-pulse ^{25}Mg MAS NMR spectra of MgO nanocubes (a) before and (b) after exposure to H_2O vapor ($p(H_2O)$ = 32 mbar) in a closed sample chamber. The spectrum of the MgO powder sample which was contacted with $SiCl_4/O_2$ and stored in a vacuum thereafter is shown as trace (c). Trace (d) corresponds to the spectrum of $Mg_3(OH)_5Cl{\cdot}4H_2O$.

that the MgO nanocubes remain essentially unaltered at this stage of sample treatment.

Exposure of chlorinated MgO nanocubes to water vapor initiates growth of $Mg_3(OH)_5Cl{\cdot}4H_2O$ needles. The ^{25}Mg NMR spectrum of this new phase (Figure 2d) shows a signal at 0 ppm. Since ^{25}Mg is a quadrupolar nucleus, its line shape also gives some information about the orientation of the nucleus in the local electric field. Narrow and symmetrical NMR resonance line of the $Mg_3(OH)_5Cl{\cdot}4H_2O$ reflects a symmetric environment of Mg in the MgO_6 octahedra. In addition, the spectrum confirms that Mg has been quantitatively incorporated into $Mg_3(OH)_5Cl{\cdot}4H_2O$.

We carried out control experiments on commercially available low surface area MgO powders (Aldrich #529699) with average domain sizes of d_{XRD} = 35 nm and found that—irrespective from whether the oxide was contacted with $SiCl_4/O_2$ prior to H_2O vapor exposure or not—the powders became only superficially transformed into the hydroxide of the brucite modification (with crystallite dimensions x_{001} and x_{110} of 28 and 25 nm, respectively. Further details in Supporting Information). The absence of needle growth as concluded from the corresponding XRD and transmission electron microscopy (TEM) data clearly underlines the critical importance of high surface-to-volume ratios for the here reported transformation process.

The associated increase in surface reactivity makes chlorinated MgO nanocubes to physicochemically dynamic materials in environmental media. Humidity, i.e., the presence of water molecules in the gas phase, is key to the growth of $Mg_3(OH)_5Cl{\cdot}4H_2O$ needles. In the presence of water vapor, the hydrolyzable Mg−O surface elements break. In a way similar to the hydrolysis and polycondensation reactions of typical sol−gel reactions, the broken Mg−O bond leads to the formation of Mg^{2+} and OH^- ions to form magnesium hydroxide, which spreads and forms thin ribbon-like films on top of the particle agglomerates. The transformation is driven by the high energy of highly dispersed chlorinated MgO/Cl_x particles and $Si_xCl_yO_z$ moieties (related experimental evidence see Supporting Information) as educts and the thermodynamic stability of the newly formed compound $Mg_3(OH)_5Cl{\cdot}4H_2O$. Figure 3 illustrates the growth mechanism.

We assume that a thin liquid layer forms on the surface of the chlorinated nanocube agglomerates and provides a new reaction medium upon contact with water vapor. The local supersaturation of dissolved ions leads to the precipitation of $Mg_3(OH)_5Cl{\cdot}4H_2O$ seeds that anisotropically grow out of the reaction pool (Figure 3) with [010] as the growth direction and the (101) plane being subject to fast material addition and growth. Further needle growth is sustained by ion transport inside the aqueous film and across the concentration gradient.

dx.doi.org/10.1021/cg500538d | Cryst. Growth Des. 2014, 14, 4236−4239

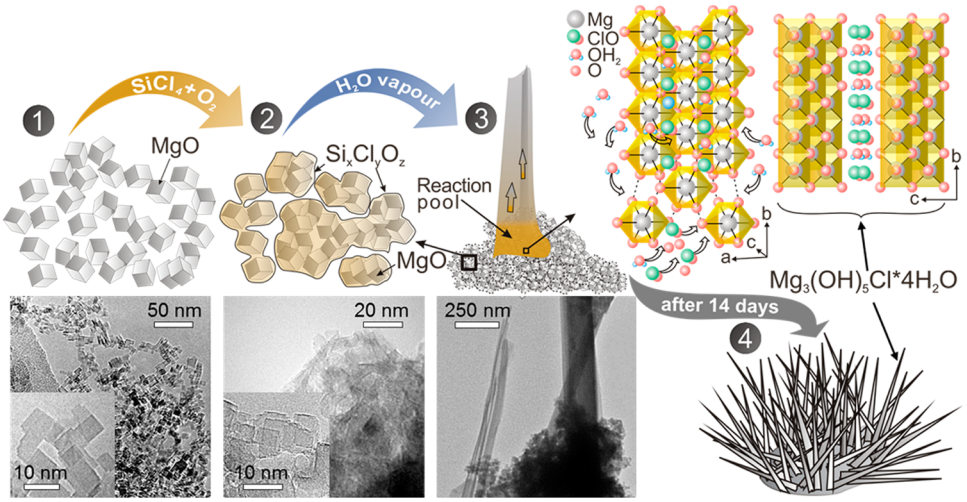

Figure 3. Schematic illustrating the growth mechanism of magnesium oxychloride fibers from MgO nanocubes kept in H_2O vapor environment. (1) MgO nanocubes; (2) MgO nanocubes covered with $Si_xCl_yO_z$ layers (experimental NMR evidence in Supporting Information); (3) $Mg_3(OH)_5Cl{\cdot}H_2O$ fibers start to grow out from the grains of chlorinated and agglomerated nanocubes (see corresponding TEM image in the inset and in the Supporting Information) as a result of contact with water vapor. (4) After 14 days, the formation of hedgehog like structures is completed.

In addition to the mechanistic scheme, Figure 3 also contains a perspective view of the crystal structure of $Mg_3(OH)_5Cl{\cdot}4H_2O$ (F5 phase). The structure corresponds to an arrangement of infinite triple chains of almost regular MgO_6 octahedra running along the *b*-axis and [010] direction as the growth direction and intercalated disordered chlorides and water molecules or hydroxides.[13] After 14 days of storage in H_2O vapor environment, the formation of hedgehog-like structures is completed. Related to the different stages of the nanostructure transformation process, representative TEM images are added. Silicon originating from the chlorine source $SiCl_4$ is neither part of the crystalline product nor does it contribute to any other crystalline phase and XRD pattern. We, therefore, expect that it remains after growth as amorphous SiO_x in the base region of the needle assembly, or, so to speak, in the pincushion.

Studies on the interplay between hydration state, microstructure, and mechanical properties of oxyhydrates revealed the growth of $Mg_3(OH)_5Cl{\cdot}4H_2O$ needles in aqueous pastes of $MgO/MgCl_2$ mixtures.[17−19] More recently material chemists reported the solution synthesis of oxychloride nanorods upon contact of nanocrystalline MgO with concentrated aqueous magnesium chloride solution.[20] As a completely novel effect, the here reported transformation process does occur in air and leads to 1-D hydroxides with interfacial regions that are susceptible to ion exchange. The overall process points to a simple and direct way to spatially control needle growth via arrangement of MgO nanocube ensembles (Figure 1a) as seeding regions. Moreover, constitutional water at the surface as well as inside the bulk structure provides additional functionality for the deposition of catalyst particles,[21] for ion insertion and exchange reactions that are critical for materials design in energy conversion technology[22−24] as well as for the development of structural materials.[19,25] From a different perspective, these results underline the substantial metastability of nanomaterials and that many unintended transformations may easily occur in both environmental and biological systems.

■ ASSOCIATED CONTENT

Ⓢ Supporting Information

Experimental details concerning the process of MgO exposure to $SiCl_4$ and the water assisted needle growth, analysis of the X-ray diffraction pattern, details and additional informations from the solid-state NMR experiments, and results from control experiments on commercial MgO. This material is available free of charge via the Internet at http://pubs.acs.org.

■ AUTHOR INFORMATION

Corresponding Authors

*(M.H.) E-mail: martin.hartmann@ecrc.uni-erlangen.de.
*(O.D.) E-mail: oliver.diwald@sbg.ac.at.

Present Address

[#]National Institute of Chemistry, Ljubljana, Slovenia.

Notes

The authors declare no competing financial interest.

■ ACKNOWLEDGMENTS

A.R.G, A.S., and O.D. are grateful for substantial support from the Austrian Science Fund (FWF-PI312/ERA Chemistry). M.H. and O.D. gratefully acknowledge the support of the German Research Foundation (DFG), which, within the framework of its "Excellence Initiative", supports the cluster of Excellence "Engineering of Advanced Materials" at the University of Erlangen-Nürnberg.

■ REFERENCES

(1) Meldrum, F. C.; Cölfen, H. *Chem. Rev.* **2008**, *108*, 4332−4432.
(2) Patzke, G. R.; Zhou, Y.; Kontic, R.; Conrad, F. *Angew. Chem., Int. Ed.* **2011**, *50*, 826−859.
(3) Chang, S.-Y.; Yang, N.-H.; Huang, Y.-C.; Lin, S.-J.; Kattamis, T. Z.; Liu, C.-Y. *J. Mater. Chem.* **2011**, *21*, 4264−4271.
(4) Peng, X.; Jin, J.; Ericsson, E. M.; Ichinose, I. *J. Am. Chem. Soc.* **2007**, *129*, 8625−8633.
(5) Finlayson-Pitts, B. J. *Phys. Chem. Chem. Phys.* **2009**, *11*, 7760.
(6) Müller, M.; Stankic, S.; Diwald, O.; Knözinger, E.; Sushko, P. V.; Trevisanutto, P. E.; Shluger, A. L. *J. Am. Chem. Soc.* **2007**, *129*, 12491−12496.
(7) Sternig, A.; Stankic, S.; Müller, M.; Siedl, N.; Diwald, O. *Nanoscale* **2012**, *4*, 7494−7500.

(8) Sternig, A.; Müller, M.; McCallum, M.; Bernardi, J.; Diwald, O. *Small* **2010**, *6*, 582−588.
(9) Sternig, A.; Klacar, S.; Bernardi, J.; Stöger-Pollach, M.; Grönbeck, H.; Diwald, O. *J. Phys. Chem. C* **2011**, *115*, 15853−15861.
(10) McKenna, K. P.; Koller, D.; Sternig, A.; Siedl, N.; Govind, N.; Sushko, P. V.; Diwald, O. *ACS Nano* **2011**, *5*, 3003−3009.
(11) Pang, H.; Ning, G.; Gong, W.; Ye, J.; Lin, Y. *Chem. Commun.* **2011**, *47*, 6317−6319.
(12) Ding, Y.; Zhang, G.; Wu, H.; Hai, B.; Wang, L.; Qian, Y. *Chem. Mater.* **2001**, *13*, 435−440.
(13) Sugimoto, K.; Dinnebier, R. E.; Schlecht, T. *Acta Crystallogr., Sect. B: Struct Sci.* **2007**, *63*, 805−811.
(14) MacKenzie, K. J. D.; Meinhold, R. H.; Sherrif, B. L.; Xu, Z. *J. Mater. Chem.* **1993**, *3*, 1263−1269.
(15) MacKenzie, K. J. D.; Meinhold, R. H. *Thermochim. Acta* **1993**, *230*, 339−343.
(16) Pallister, P. J.; Moudrakovski, I. L.; Ripmeester, J. A. *Phys. Chem. Chem. Phys.* **2009**, *11*, 11487.
(17) Matkovic, B.; Popovic, S.; Rogic, V.; Zunic, T.; Young, J. F. *J. Am. Ceram. Soc.* **1977**, *60*, 504−507.
(18) Montle, J. F.; Mayhan, K. G. *J. Fire Flammability/Fire Retard. Chem.* **1974**, *1*, 243−254.
(19) Chau, C. K.; Li, Z. *Adv. Cem. Res.* **2008**, *20*, 85−92.
(20) Jeevanandam, P.; Mulukutla, R. S.; Yang, Z.; Kwen, H.; Klabunde, K. J. *Chem. Mater.* **2007**, *19*, 5395−5403.
(21) Brown, M. A.; Carrasco, E.; Sterrer, M.; Freund, H.-J. *J. Am. Chem. Soc.* **2010**, *132*, 4064−4065.
(22) Goodenough, J. B. *Acc. Chem. Res.* **2013**, *46*, 1053−1061.
(23) Singh, K.; Nowotny, J.; Thangadurai, V. *Chem. Soc. Rev.* **2013**, *42*, 1961.
(24) Fabbri, E.; Pergolesi, D.; Traversa, E. *Chem. Soc. Rev.* **2010**, 39.
(25) Young, M. *Nature* **1974**, *250*, 443.